Supporting Information

Role of polymer donor side-chain length on formation and processing of waterborne nanoparticles for organic solar cells.

Hugo Laval[#*], Martina Rimmele[#*], Alberto Peinador Veiga, Xabier Rodríguez-Martínez, Gilles Pécastaings, Marc Schmutz, Alejandro Salinas-Villasenor, Christine Lartigau-Dagron, Antoine Bousquet, Guillaume Wantz, Jaime Martin, Martin Heeney, Sylvain Chambon*

[#] Authors contributed equally

Dr Hugo Laval, Dr Guillaume Wantz, Dr Sylvain Chambon
Université de Bordeaux, CNRS, Bordeaux INP, IMS, UMR 5218, F-33400 Talence, France.

Dr Martina Rimmele, Prof Martin Heeney
Department of Chemistry and Centre for Processable Electronics, Imperial College London, London W12 0BZ, United Kingdom.

Alberto Peinador Veiga, Dr Xabier Rodríguez-Martínez, Dr Jaime Martin
Universidade da Coruña, Campus Industrial de Ferrol, CITENI, Campus de Esteiro S/N, 15471 Ferrol, Spain.

Dr Jaime Martin
Oportunius Programme, Axencia Galega de Innovacion, Xunta de Galicia, Galicia (Spain)

Dr Gilles Pécastaings, Univ. Bordeaux, CNRS, CRPP, UMR 5031, F-33600 Pessac, France

Dr Marc Schmutz
Université de Strasbourg, CNRS, Institut Charles Sadron, PLAMICS, F67000 Strasbourg, France

Alejandro Salinas-Villasenor, Dr Christine Lartigau-Dagron, Dr Antoine Bousquet,
Universite de Pau et Pays de l'Adour, CNRS, IPREM, Pau, France.

Prof Martin Heeney
King Abdullah University of Science and Technology (KAUST), Thuwal, 23955–6900, Saudi Arabia

*Corresponding author email: hlaval-iis@g.ecc.u-tokyo.ac.jp, martina.rimmele@imperial.ac.uk, sylvain.chambon@u-bordeaux.fr

Table of Contents

1. Methods

Materials: Chloroform (≥99%), ethanolamine (≥99.5%), ethanol (≥99.8%), zinc acetate dihydrate, sodium dodecyl sulfate (SDS) were purchased from Sigma Aldrich. Deionized water was obtained from a PURELAB Flex system (≈15 MΩ). MoO_3 powder was purchased from NEYCO. Donor polymers FO4-T, FO6-T and FO8-T were synthesized according to previously reported procedures.[1] Acceptor small molecule Y6 was purchased from Brilliant Matters. All the materials were used as received without further purification.

High-temperature GPC**:** High-temperature gel permeation chromatography (HT-GPC) measurements were carried out on an Agilent 1260 II High-Temperature GPC System fitted with three Agilent PLgel 10 μm MIXED-B, 7.5 x 300 mm columns, RID and HTELSD detectors, using HPLC-grade 1,2,4-trichlorobenzene (with 0.0125% BHT inhibitor) as eluent at a flow rate of 1.0 mL min^{-1} and temperature of 150°C. Number average molecular weight (M_n), weight average molecular weight (M_w), and dispersity (*Đ*) values are reported relative to poly(styrene) standards that were run at the same temperature. Samples were prepared to a concentration of approximately 1 mg mL^{-1} in the same solvent as the eluent.

Nanoparticle Synthesis: Water-based inks were obtained with mini- emulsion synthesis. For the organic phase, a total of 35 mg ml^{-1} of FOX-T:Y6 (wt% of 1:1.5) mixture was first dissolved in chloroform and

stirred for 2 h at 65 °C in a nitrogen-filled glovebox. Aqueous phases were obtained by dissolving 5 mg ml^{-1} of SDS in deionized water and stirred for 30 min at RT. A macro-emulsion was then obtained by adding the organic phase into the aqueous phase with 1:5 volume ratio and stirring for 1 h at 40 °C (1000 rpm). The mini-emulsion dispersion was formed by sonicating the macro-emulsion using a BRANSON Digital Sonifier 450 in an ice-water bath for 2 min at 15% of the maximum power in an ice-water bath. Chloroform evaporation was completed by stirring the miniemulsion 3 h at 65 °C. To eliminate the excess SDS, the centrifugal step was carried out by using Amicon Ultra-15 centrifuge filters (cut-off 100 kDa) and a Hettich Universal 320 centrifugal. Five centrifugation cycles were done at 3500 rpm for 5 min. The retentate was raised to 15 mL with MilliQ water between each step. Final aqueous dispersions were obtained with a concentration of 60 mg ml^{-1} of active materials.

OSCs Fabrication: OPV devices were fabricated with an inverted architecture glass/ITO/ZnO/active layer/MoO_3/Ag, where ZnO and MoO_3 were used as electron transport (ETL) and hole transport (HTL) interlayers, respectively. The ITO covered glasses (1.5 × 1.5 cm^2,10 Ω/□, VisionTek) were cleaned by sequential ultrasonic treatments: diluted soap Hellmanex III, deionized water and isopropanol. The ZnO precursor solution was prepared by mixing zinc acetate dihydrate (165 mg) and ethanolamine (90 μL) with ultrapure ethanol (5 mL). The solution was then stirred at 55 °C in air for 30 min and left at room temperature under continuous stirring prior to deposition. Before depositing the ETL, the substrates were dried and treated by UV-O_3 for 15 min. ZnO precursor solution was then spin-coated to form 40 nm thin films. The substrates were then thermally annealed in air at 180 °C for 30 min. Prior the np-BHJ active layers deposition, ZnO substrates were treated by UV-O_3 for 20 min to increase the hydrophilicity of the surface. The colloidal dispersions were then spin-coated onto the HTL with a rotation speed of 3000 rpm and subsequently annealed at various temperatures in a nitrogen-filled glovebox. Afterward, vacuum evaporation ($P = 10^{-6}$ mbar) was used to deposit HTL MoO_3 (7 nm thick with a rate of 0.5 Å s^{-1}) and electrode Ag (80 nm thick with a rate of 2 Å s^{-1}). The area of OPV devices was 10.5 mm^2.

Current-Voltage Characterization: A solar simulator using a xenon source and AM 1.5 G filters (Newport LCS-100) was used. The light intensity of the lamp was set at 100 mW cm^{-2} using a calibrated silicon reference cell from Newport Co. The J-V curves were recorded in the dark and under 1-sun using

a Keithley 2400 SMU, and parameters were directly extracted via a LabVIEW program. J-V characterization was done in a nitrogen-filled glovebox.

External Quantum Efficiency: EQE measurements were carried out using a PVE300 Photovoltaic EQE from Bentham Co. EQE was performed in an ambient atmosphere and all OPV devices were encapsulated. J-V curves were re-recorded afterward to verify the good encapsulation.

Differential scanning calorimetry (DSC): DSC measurements were performed on a DSC 3, Mettler Toledo STAR® system under a nitrogen atmosphere. For each sample, the temperature was increased at 10°C min^{-1} from 25°C to 250°C for nanoparticles and to 320°C for other samples, then cooled down to 25°C following the same ramp. Two kinds of samples were analyzed, pure Y6 and blends FOX-T:Y6 solubilized in chloroform and then dropped in the crucible and evaporated several times to accumulate enough material. Nanoparticles were analyzed after an extensive freeze-drying of the dispersions to remove water. For nanoparticle dispersions, only one cycle was performed, representative of the processing conditions used during device preparation.

Atomic Force Microscopy: AFM images were acquired with a Bruker Icon microscope using Peakforce tapping mode with ScanAsyst-Air probes (Bruker). 2 µm x 2 µm and 500 nm x 500 nm images were acquired at a resolution of 512 x 512 pixels with scan rates between 0.5 Hz and 1.5Hz.

Grazing Incidence Wide-Angle X-ray Scattering (GIWAXS): GIWAXS experiments were performed at the NCD-SWEET beamline at ALBA Synchrotron using an X-ray beam of 12.4 keV at an angle of incidence of 0.12º. Samples were illuminated for 1 s (in air) to avoid photodegradation. Scattering patterns were acquired using a Rayonix LX255-HS detector positioned at 204.84 mm from the samples and calibrated with a Cr_2O_3 standard. The diffractograms were corrected by subtracting 30% of the intensity attributed to the air background (baseline). They were then converted to the reciprocal space using pyFAI. The linecuts were extracted for the azimuthal regions χ = 0-45º (out-of-plane, oop) and χ = 45º-90º (in-plane, ip). The diffraction peaks were fitted according to Pseudo-Voigt lineshapes while using an exponential decay and a linear function as background.

Cryo-TEM: The principle of Cryo-TEM of vitrified specimens was previously described by Dubochet *et al.* in 1988. The vitrification of the samples was carried out in a homemade vitrification system. The chamber was maintained at 22 °C, and the relative humidity was 80%. A 5 µL drop of the sample was

deposited onto a lacey carbon film covered with a 300 mesh Cu grid (Ted Pella-USA) rendered hydrophilic using an ELMO glow discharge unit (Cordouan Technologies, Pessac, France). The grid was automatically blotted to form a thin film and plunged in liquid ethane at -190 °C, as maintained by liquid nitrogen. Thus, a vitrified film was obtained in which the native structure of the nanoparticles was preserved. The grid was mounted onto a cryo holder (Gatan 626-Pleasanton, CA, USA) and observed under low-dose conditions (10 e A^2) in a Tecnai G2 microscope (FEI, Eindhoven, Netherlands) at 200 kV. Images were acquired using an Eagle slow scan CCD camera (FEI).

UV-Visible-NIR Spectrophotometry: UV-vis-NIR absorption spectra were acquired on a JASCO V-570 spectrophotometer from 300 to 1000 nm with 0.5 nm step.

Photoluminescence Spectrophotometry: Photoluminescence spectra were acquired on a JASCO FP-8700 spectrophotometer. Excitation wavelength was set at 624 (or 820) nm and emission was recorded from 650 (or 850) to 1400 nm with a step of 2 nm and a scan speed of 5000 nm min^{-1} with 10 repetitions.

2. Polymer Characterisation

The polymers FO4-T, FO6-T and FO8-T were prepared according to our previously published protocol.[1] The molecular weights were determined using high temperature gel permeation chromatography (HT-GPC) with 1,2,4-trichlorobenzene at 150 °C against poly(styrene) standards.

Table S1. GPC results for polymers FO4-T, FO6-T and FO8-T at 150 °C in 1,2,4-trichlorobenzene.

	M_n (kDa)	M_w (kDa)	*Đ*
FO4-T	17.5	45.8	2.61
FO6-T	29.0	72.0	2.48
FO8-T	19.6	49.2	2.51

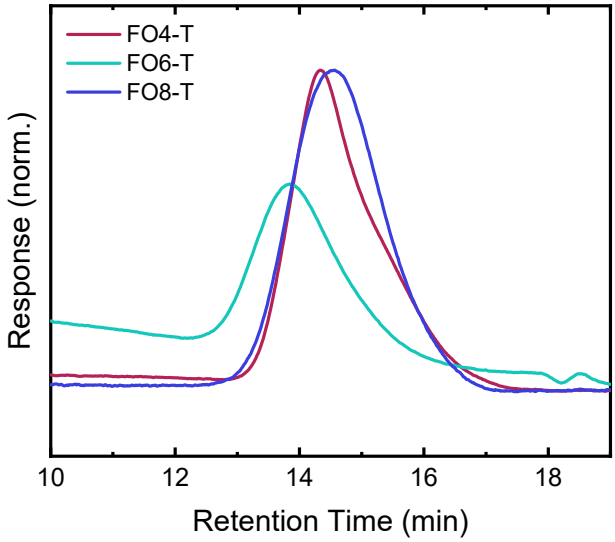

Figure S1. GPC traces of FO4-T, FO6-T and FO8-T in 1,2,4-trichlorobenzene at 150 °C.

3. Nanoparticle Characterisation

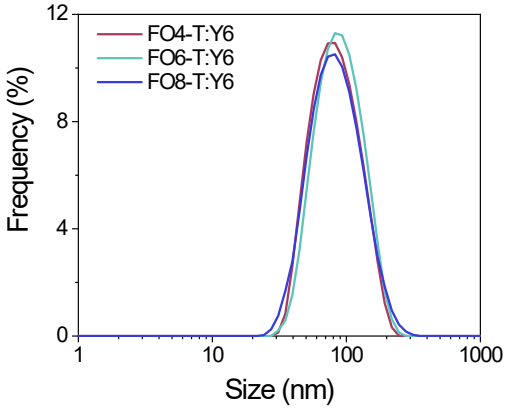

Figure S2. Size distributions for FO4-T:Y6, FO6-T:Y6 and FO8-T:Y6 np-BHJ dispersed in water measured by a dynamic light scattering method.

Table S2. Average diameter and standard deviation of FO4-T:Y6, FO6-T:Y6 and FO8-T:Y6 np-BHJ dispersed in water measured by a dynamic light scattering method. (average obtained from 5 measurements).

np-BHJ	FO4-T:Y6	FO6-T:Y6	FO8-T:Y6
Z-average (nm)	58 ± 1	59 ± 1	61 ± 2

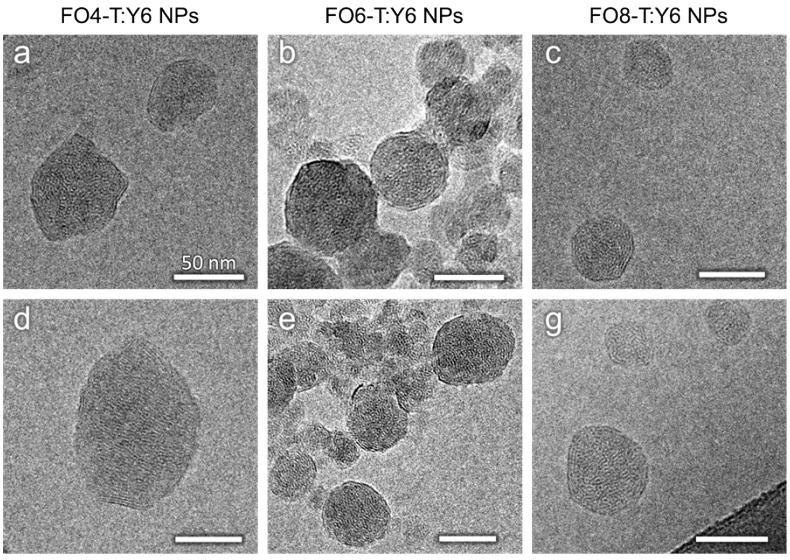

Figure S3. Cryo-TEM images of FO4-T:Y6 (a,d), FO6-T:Y6 (b,e) and FO8-T:Y6 (c,g) nanoparticles.

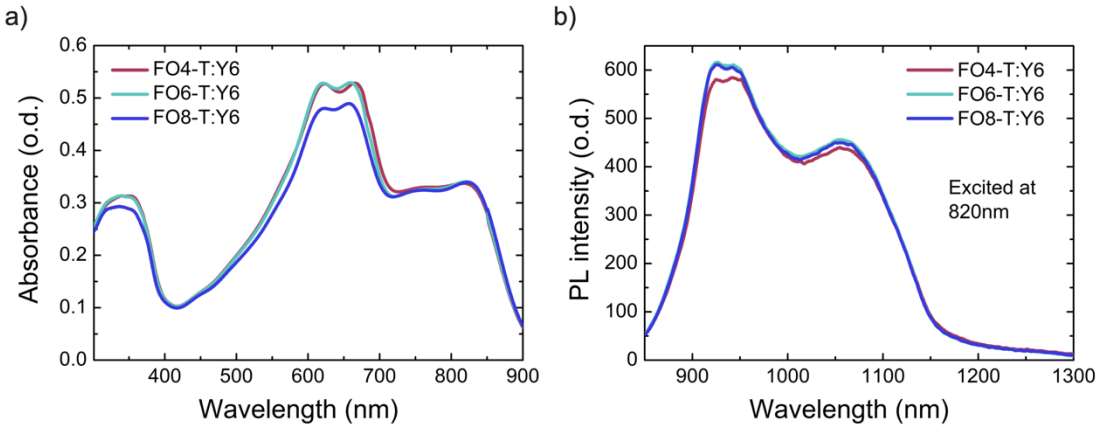

Figure S4. (a) UV-visible absorption and (b) PL spectra of FO4-T:Y6, FO6-T:Y6, FO8-T:Y6 nanoparticles dispersions. The wavelength of the PL excitation was set at 820nm.

4. Device Characterisation

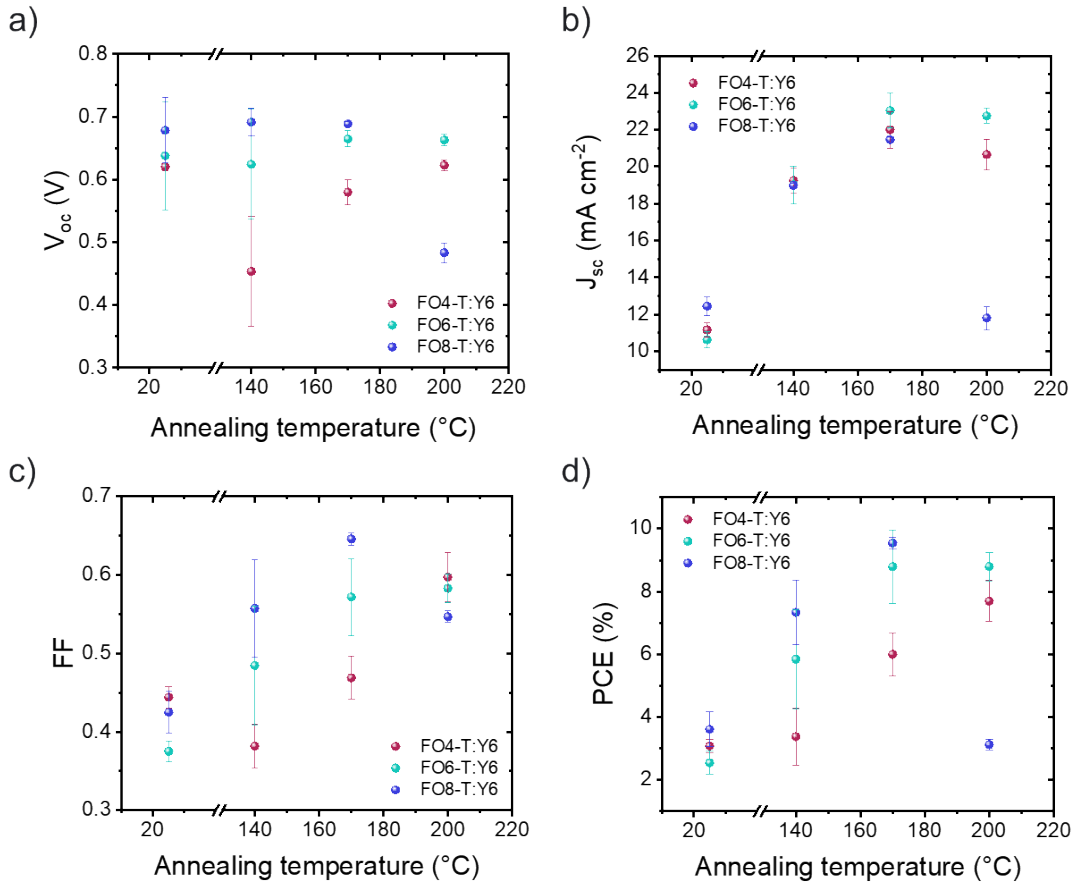

Figure S5. Photovoltaic characteristics for FO4-T:Y6, FO6-T:Y6 and FO8-T:Y6 np-BHJ OPV devices. Average values and standard deviation are calculated on 4 to 8 devices.

Table S3. Photovoltaic performances of optimized FOx-T:Y6 np-BHJ and their optimal thermal annealing temperature. Average over 8 devices. Hero cell in brackets.

	Thermal annealing temperature (°C)	J_{sc} (mA.cm^{-2})	V_{oc} (V)	FF	PCE (%)
FO4-T:Y6	200°C	22.43 ± 0.43 (22.25)	652 ± 12 (670)	0.62 ± 0.01 (0.63)	9.01 ± 0.27 (9.45)
FO6-T:Y6	200°C	22.33 ± 0.83 (23.42)	656 ± 14 (657)	0.62 ± 0.02 (0.63)	9.05 ± 0.34 (9.88)
FO8-T:Y6	170°C	24.17 ± 0.48 (24.78)	707 ± 4 (713)	0.61 ± 0.01 (0.60)	10.40 ± 0.17 (10.64)

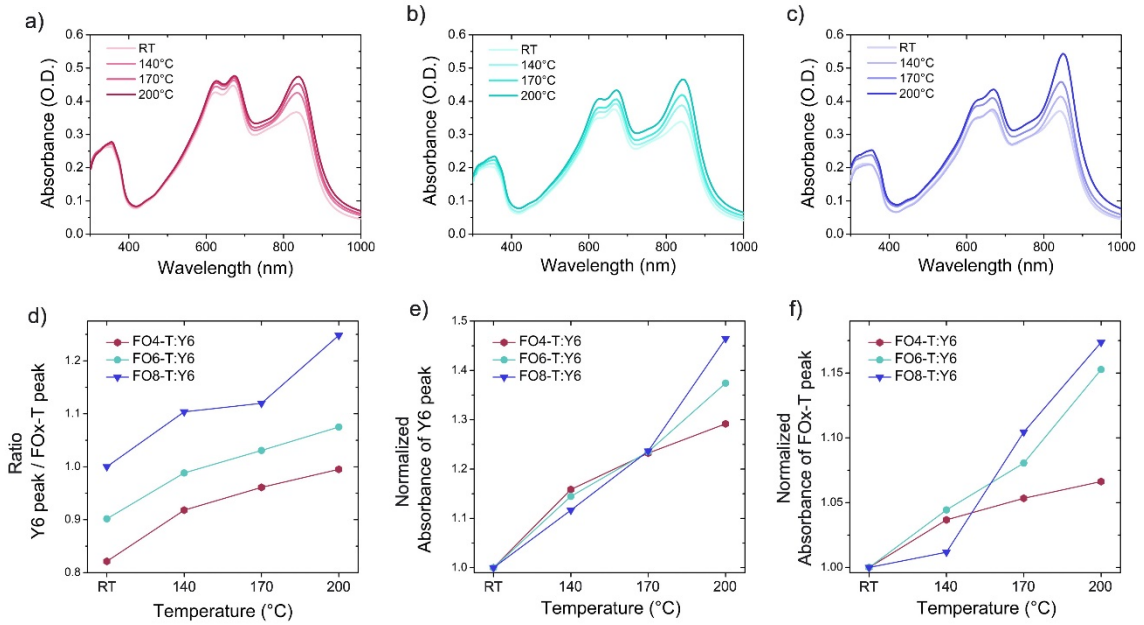

Figure S6. UV-visible absorption spectra of (a) FO4-T:Y6 np-BHJ films, (b) FO6-T:Y6 np-BHJ films and (c) FO8-T:Y6 np-BHJ films with varying thermal treatment. Evolution of (d) the ratio between the peak intensity of Y6 (at 840 nm) and FOx-T (at 675 nm) with varying temperature and the peak intensity of (e) Y6 and (f) FOx-T with varying temperature.

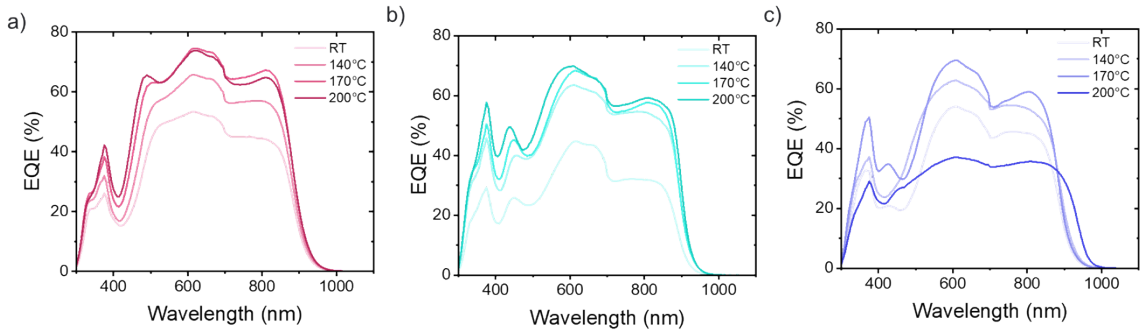

Figure S7. External quantum efficiency (EQE) spectra of a) FO4-T:Y6, b) FO6-T:Y6 and c) FO8-T:Y6 the three blends at different thermal annealing temperature.

5. Thermal Characterisation

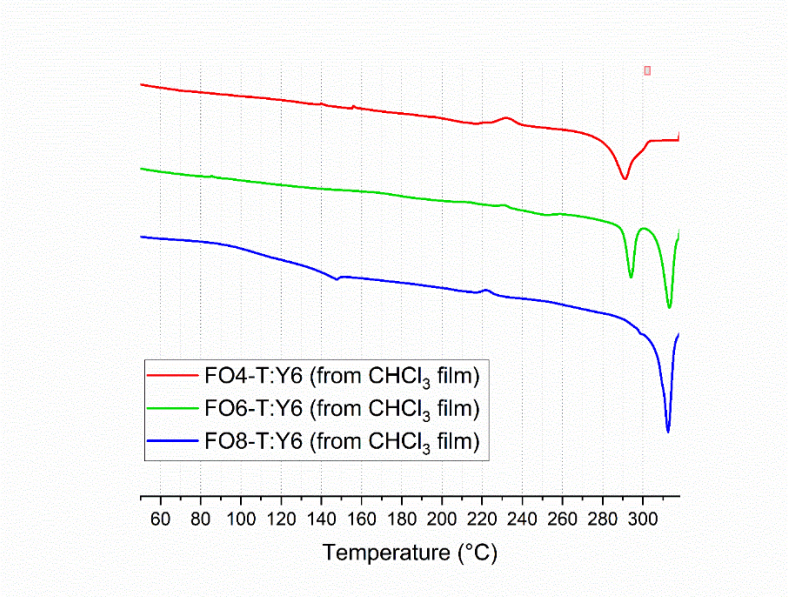

Figure S8. DSC thermographs of films composed of FO4-T, FO6-T and FO8-T blended with Y6 (heating cycle, exo up).

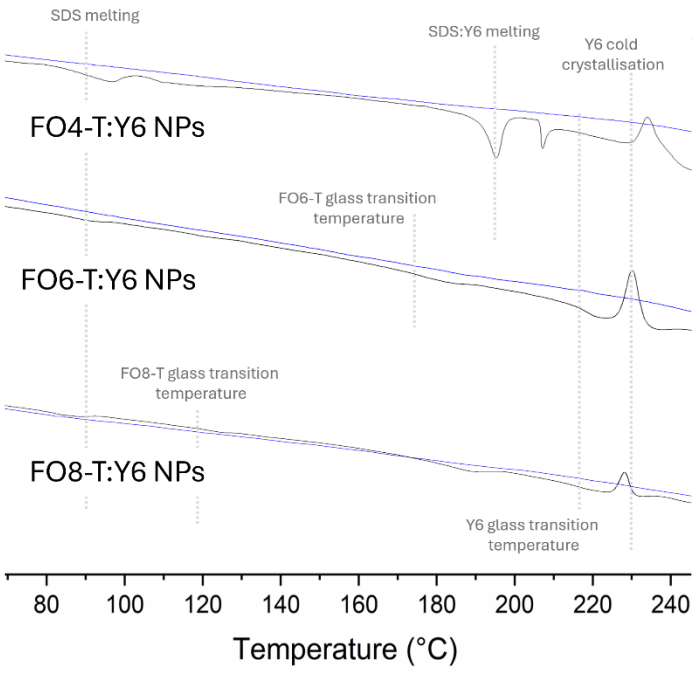

Figure S9. DSC thermograms of NPs of polymers FO4-T, FO6-T and FO8-T blended with Y6 (heating cycle, exo up).

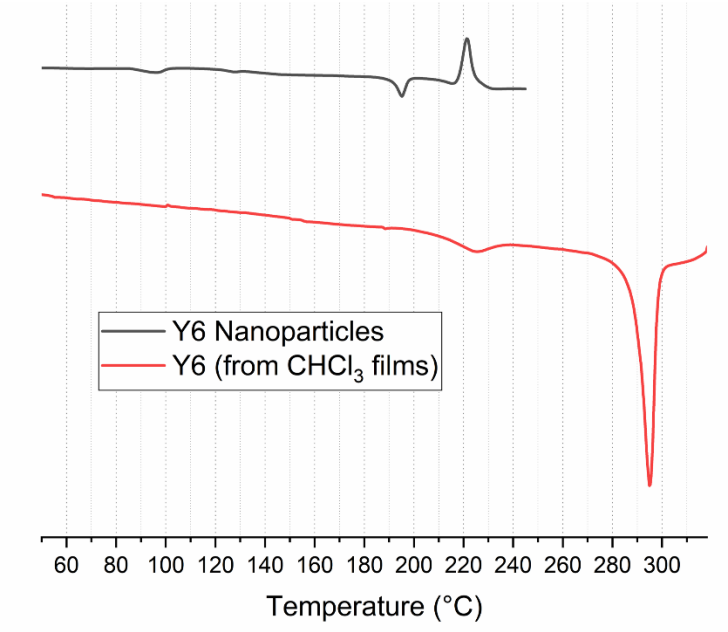

Figure S10. DSC thermograms for Y6 films and NPs (heating cycle, exo up).

6. Morphological Characterisation

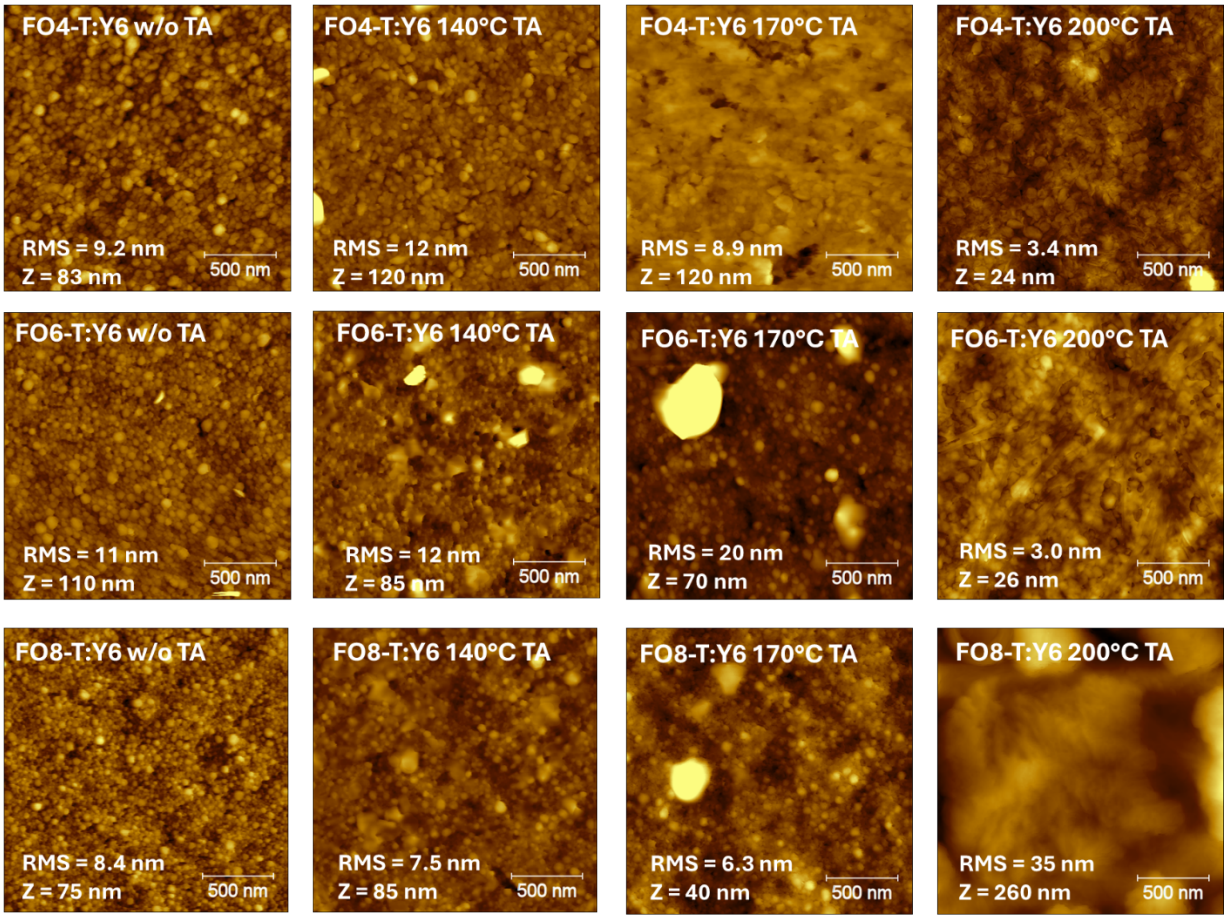

Figure S11. AFM topographic images of FOX-T:Y6 blends at different annealing temperatures at a scale of 2 µm x 2 µm.

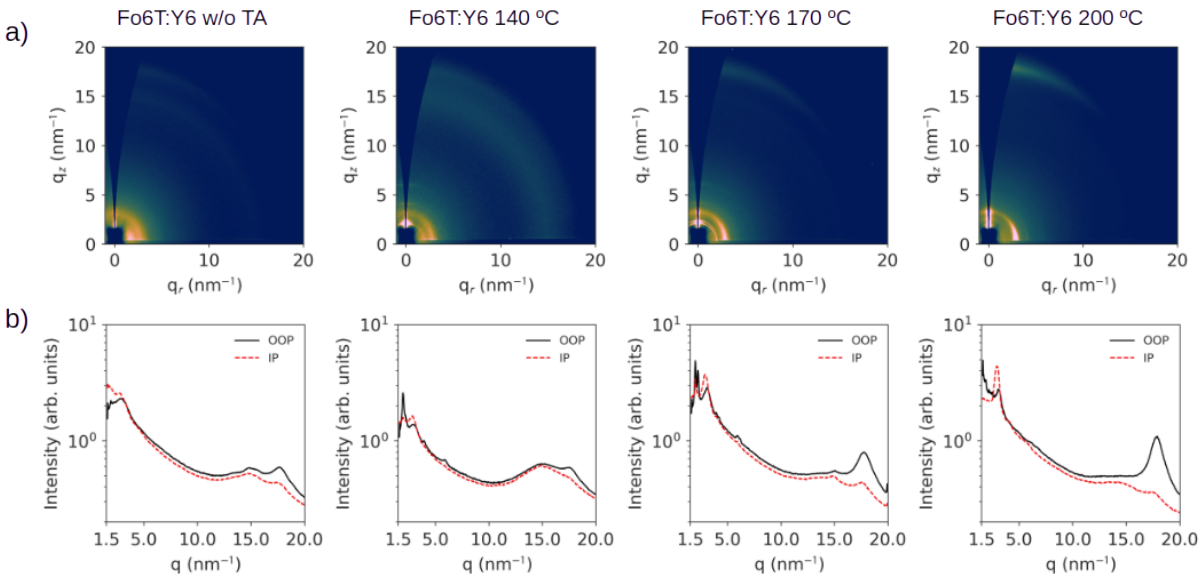

Figure S12. Morphological characterization of NP films of FO6-T:Y6. a) 2D GIWAXS patterns and b) 1D line plots of FO6-T:Y6 films annealed at different temperatures.

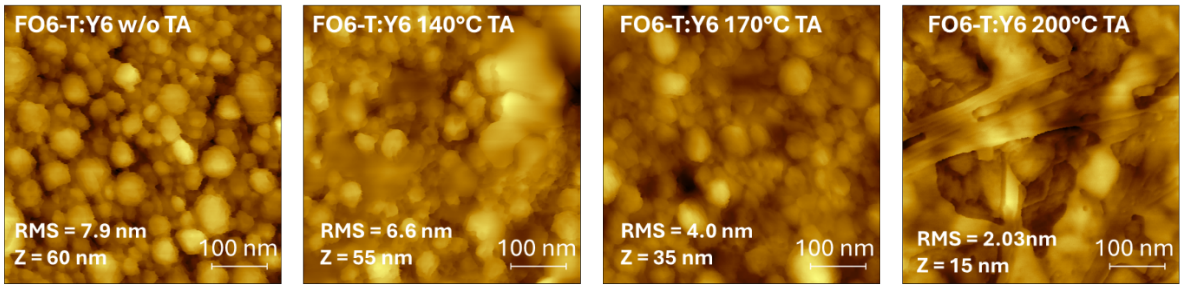

Figure S13. AFM images of FO6-T:Y6 blends annealed at different temperatures.

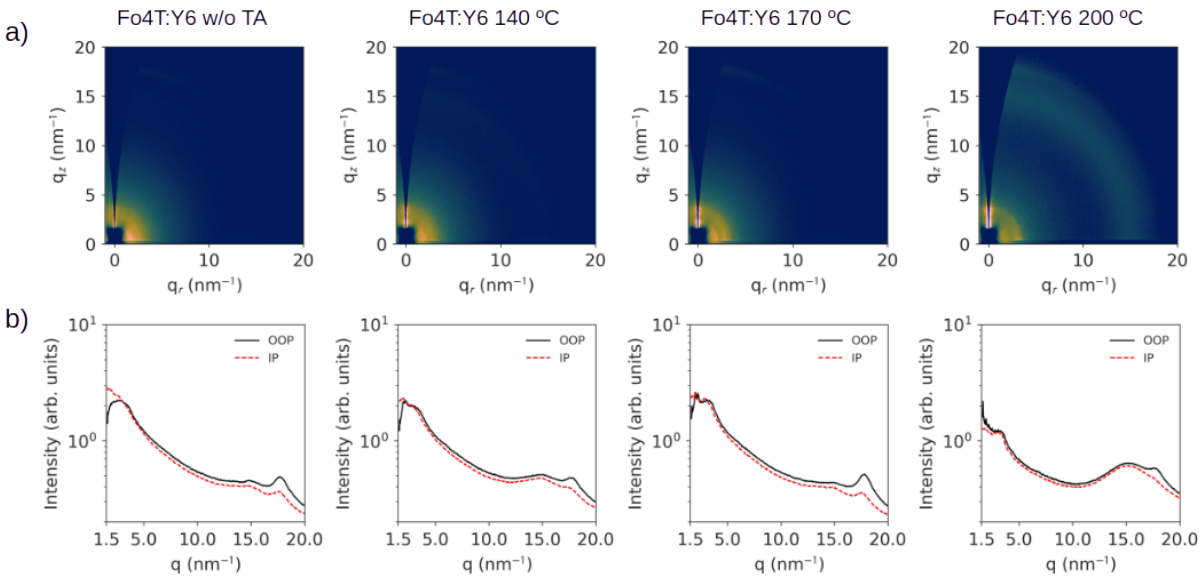

Figure S14. Morphological characterization of NP films of FO4-T:Y6. a) 2D GIWAXS patterns and b) 1D line plots of FO4-T:Y6 films annealed at different temperatures.

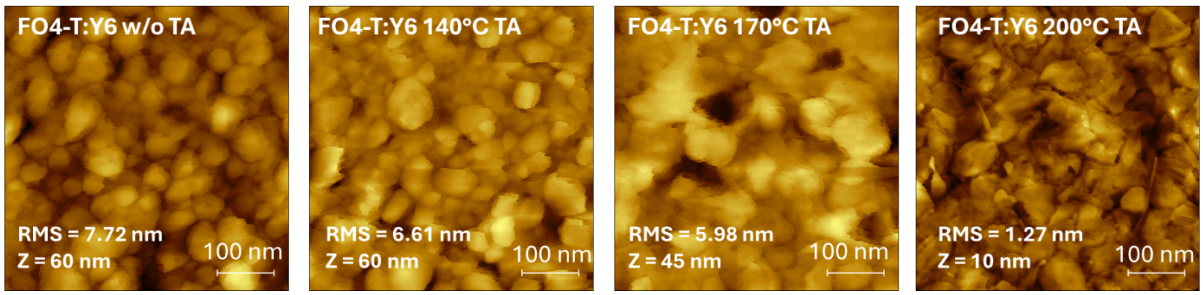

Figure S15. AFM topographic images of FO4-T:Y6 blends annealed at different temperatures.

Table S4. GIWAXS characterization for blend NPs for the (100) plane, here ascribed to the lamellar stacking of the polymer.

	TA	**Center (nm^{-1})**	**d (nm)**	**FWHM (nm^{-1})**	**g**	**CCL (nm)**
FO4-T:Y6	w/o	3.36	1.87	1.37	0.25	4.1
	140 °C	2.99	2.10	1.81	0.31	3.1
	170 °C	3.14	2.00	1.53	0.28	3.7

	200 °C	3.31	1.90	0.88	0.21	6.5
FO6-T:Y6	w/o	2.90	2.17	1.32	0.27	4.3
	140 °C	2.91	2.16	0.95	0.23	6.0
	170 °C	2.98	2.11	0.69	0.19	8.1
	200 °C	2.95	2.13	0.74	0.20	7.7
FO8-T:Y6	w/o	2.71	2.32	1.34	0.28	4.2
	140 °C	2.76	2.28	0.75	0.21	7.5
	170 °C	2.85	2.20	0.50	0.17	11.3
	200 °C	2.89	2.17	0.59	0.18	9.5

Table S5. GIWAXS characterization for blend NPs for the π-π stacking reflection, resulting from a convolution of the (010) planes of the polymer and the π-stacking of Y6.

	TA	**Center (nm^{-1})**	**d (nm)**	**FWHM (nm^{-1})**	**g**	**CCL (nm)**
FO4-T:Y6	w/o	17.78	0.35	1.94	0.13	2.9
	140 °C	17.95	0.35	1.90	0.13	3.0
	170 °C	17.86	0.35	1.74	0.12	3.3
	200 °C	18.10	0.35	1.75	0.12	3.2
FO6-T:Y6	w/o	17.63	0.36	2.83	0.16	2.0
	140 °C	17.71	0.35	2.45	0.15	2.3
	170 °C	17.81	0.35	1.73	0.12	3.3
	200 °C	17.87	0.35	1.62	0.12	3.5
FO8-T:Y6	w/o	17.88	0.35	2.95	0.16	1.9
	140 °C	17.77	0.35	1.89	0.13	3.0
	170 °C	17.78	0.35	1.56	0.12	3.6
	200 °C	17.95	0.35	1.42	0.11	4.0

7. References

1. M. Rimmele, Z. Qiao, J. Panidi, F. Furlan, C. Lee, W. L. Tan, C. R. McNeill, Y. Kim, N. Gasparini and M. Heeney, *Materials Horizons*, 2023, **10**, 4202-4212.